A Multiscale Assessment of the Springtime U.S. Mesoscale Convective Systems in the NOAA GFDL AM4

Zhenyu You[1], Yi Deng[1], Yi Ming[2], Wenhao Dong[3,4]

Corresponding authors: Zhenyu You, zyou35@gatech.edu; Yi Deng, yi.deng@eas.gatech.edu

1 School of Earth and Atmospheric Sciences, Georgia Institute of Technology, 311 Ferst Drive, Atlanta, GA 30332-0340, USA

2 Department of Earth and Environmental Sciences, Boston College, Chestnut Hill, MA, USA

3 NOAA/Geophysical Fluid Dynamics Laboratory, Princeton, NJ, USA

4 Cooperative Programs for the Advancement of Earth System Science, University Corporation for Atmospheric Research, Boulder, CO, USA

Abstract

This study presents a multiscale assessment of the springtime U.S. Mesoscale Convective Systems (MCSs) in the NOAA Geophysical Fluid Dynamics Laboratory (GFDL)'s Atmosphere Model version 4 (AM4). In AM4, MCSs exhibit lower intensity but longer duration, producing more precipitation compared to observation. The overall MCS activity demonstrates a "location bias" with its peak shifting from the Southern Great Plains to the Midwest in AM4, causing an eastward shift in associated precipitation. However, the dry bias of MCS precipitation over the Great Plains due to this shift is compensated by additional precipitation from amplified extratropical cyclone activities. Further analysis reveals that AM4 effectively reproduces the spatiotemporal distribution and relative frequency contribution of large-scale forcing patterns driving MCS genesis. The MCS location bias emerges under all forms of large-scale forcing patterns and is further attributed to local dynamic and thermodynamic factors including weaker surface lows, eastward-shifted fronts, and suppressed low-level jets (LLJs). Here we argue that the MCS location bias results from AM4 biases in both synoptic-mesoscale anomalies (i.e., fronts and LLJs) and seasonal mean circulations. The lack of two-way air-sea interaction in AM4 creates a hemispheric-scale sea level pressure bias, which is ultimately responsible for a seasonal mean northerly bias in lower-tropospheric winds and the subsequent weakening of LLJs. The existence of such biases in prescribed sea surface temperature (SST) experiments implies the need for extra caution when utilizing extended-range forecasts for MCSs over the continental U.S.

Keywords

Mesoscale convective systems, Global climate models, Precipitation, Multiscale forcing

1. Introduction

Global climate models (GCMs) commonly exhibit warm and dry biases over the central U.S. during the boreal warm season (March-August) (e.g., Van Weverberg et al. 2018). Klein et al. (2006) argue that such biases originate from the lack of extreme precipitation events in models, leading to excessive downwelling shortwave radiation and enhanced surface heating. Less convective rainfall also reduces soil moisture, which exacerbates the excessive heating of the surface (Lin et al. 2017). The warm and dry biases are intrinsically accentuated by the difficulties in simulating warm season Mesoscale Convective Systems (MCSs), a long-standing issue in numerous GCMs (e.g., Ferraro et al. 2017; Feng et al. 2021; Lin et al. 2022).

MCSs are the most substantial type of convective storms characterized by aggregated deep convective towers and extensive stratiform regions – a unique structure distinct from scattered or isolated convective systems (Houze 2018). During the boreal warm season, MCSs are ubiquitous over the central U.S., accounting for 30-70% of the total warm season rainfall (Haberlie and Ashley 2019; Feng et al. 2019) and an even greater portion of extreme rainfall events (Schumacher and Johnson 2006). In recent decades, MCSs over the central U.S. have increased in both occurrence frequency and intensity (Feng et al. 2016). This trend is projected to continue in a warming climate (Prein et al. 2017).

Simulation of MCSs is notoriously difficult due to the complexities of their physics and dynamics, which challenge conventional convection parameterizations. Although mature MCSs span thousands of square kilometers, they are initiated as isolated deep convective cells that grow upscale to mesoscale systems with organized structures. Representing both the initiation of convective cells and the subsequent growth into MCSs poses difficulties for current GCMs (Randall et al. 2016). Much effort has been undertaken to parameterize the effects of MCSs (e.g., Mapes et al. 2006; Feng et al. 2018), but those parameterization schemes often struggle to represent the coupling between cumulus processes and low-level environment (Moncrieff et al. 2017). Consequently, GCMs, even with parameterized mesoscale convection, generally underestimate MCS activity and the associated extreme weather events (e.g., Feng et al. 2021; Lin et al. 2022).

Accurately simulating MCSs in models requires not only parameterizing complex physics of convection but also faithfully representing the *multiscale forcing mechanisms* that modulate an MCS's lifecycle. These mechanisms operate across a wide range of scales, from planetary-scale flow anomalies and synoptic-scale circulation patterns (e.g., troughs and ridges) to local dynamic and thermodynamic factors (e.g., fronts, low-level jets, atmospheric stability). Specifically, MCSs are triggered by lifting motions ahead of large-scale troughs associated with atmospheric disturbances of various dynamical origins (You and Deng 2022, referred to hereafter as YD22). The precise location of MCS genesis is further determined by local dynamic and thermodynamic factors including low-level jet (LLJ), frontal lifting, and convective instability. It remains uncertain whether GCMs can effectively simulate the large-scale forcing patterns favoring MCS geneses (e.g., Song et al. 2019). GCMs have also struggled to accurately reproduce smaller-scale factors such as the Great Plain LLJs that supply moisture for MCS development (Feng et al. 2021; Lin et al. 2022). Inaccurate representation of these multiscale forcing elements raises doubts on GCMs' capability to faithfully simulate MCSs and the associated hazards including extreme winds and heavy precipitation. Biases in MCS

activity and variability further reduce the skill of rainfall and drought predictions across subseasonal-to-seasonal (S2S) timescales at regions where MCSs play a central role in the hydrological cycle.

Given the multiscale nature of the mechanisms shaping MCS lifecycles, it is crucial to approach the evaluation of model MCS from a multiscale perspective. A systematic examination of relevant processes operating at different spatiotemporal scales facilitates the more efficient identification of the sources of model biases. For instance, YD22 shows that the positive trend of springtime MCSs over the central U.S. is largely tied to a specific pattern of large-scale forcing modulated by the Pacific Decadal Oscillation (PDO). Therefore, failures to capture this trend in a GCM may ultimately come from biases in its representation of the decadal variability in the North Pacific. Similarly, model biases in local, smaller-scale factors such as fronts and LLJs can be connected to errors in the simulated MCS genesis locations and tracks. This multiscale framework of model MCS assessment has so far received limited attention in the literature. Recognizing the potential of this approach, here we conduct a pilot study that examines MCS statistics and behavior in a 50-km resolution GCM from a multiscale perspective. Section 2 describes the atmospheric GCM, the MCS detection algorithm, and the clustering analysis used for the classification of forcing patterns. Section 3 compares the simulated MCSs, precipitation and multiscale forcing with those in observation, and reveals the potential sources of identified model biases. Section 4 provides further discussions and concluding remarks.

2. Methods

2.1. Model description

This study evaluates MCSs in a moderately high-resolution (~50 km) version of the Geophysical Fluid Dynamics Laboratory (GFDL)'s Atmosphere Model version 4 (AM4) (Zhao 2020). AM4 is the atmospheric component of the GFDL coupled physical climate model CM4, GFDL's contribution to Phase 6 of the Coupled Model Intercomparison Project (Zhao et al. 2018). It has been developed specifically to improve the simulation of regional precipitation patterns and extreme events like MCSs (Dong et al. 2021, 2023). The historical (1950-2014) climate simulation used in this analysis is driven by the observed SST and sea ice, greenhouse gases, and natural and anthropogenic aerosol emissions. Limited by the availability of the observed brightness temperature for MCS detection, the evaluation is carried out only for the period of springtime 2000-2014.

2.2. MCS detection

The MCS detection domain in this study covers most of the central U.S. (30° - 50°N, 80° - 105°W). MCSs in observation are identified from the NCEP-CPC merged geostationary satellite infrared brightness temperature (T_b) data with an approximate 4-km spatial resolution and a 30-min temporal resolution (Janowiak et al. 2001). T_b is not directly available from AM4's output, but can be inferred rather accurately from 3-hourly outgoing longwave radiation (OLR) through the following empirical formula (Dong et al. 2021, 2023):

$$\begin{cases} T_F = T_b(a + bT_b) \\ OLR = \sigma {T_F}^4 \end{cases} \quad (1)$$

where T_F is the flux equivalent brightness temperature, $\sigma = 5.67\times10^{-8}$ $Wm^{-2}K^{-4}$ is the Stefan-Boltzmann constant, and a and b are empirical coefficients based on regression. We set a at 1.223 and b at -1.106×10^{-3} K^{-1} following Ellingson and Ferrado (1983) and Dong et al. (2021).

The "detect and spread" approach is adopted to identify MCSs from the T_b datasets in both observation and AM4. The idea of this approach is to identify "cold cores" below a certain T_b threshold as individual cloud clusters and to spatially spread each cloud until a warmer threshold is met. In both AM4 and observations, a cold core is defined as continuous areas with $T_b < 221$ K and expands into a cloud cluster until T_b reaches a warmer threshold of 231 K (YD22). A cloud cluster will be pinpointed as a cold cloud system (CCS) if its area exceeds 50,000 km^2. If, between two successive T_b images, two CCSs overlap by more than 50 % going *either* forward *or* backward in time, these two CCSs are considered as the same system and the track is extended. An MCS is defined as a CCS lasting for at least 6 hours. All the detected MCS tracks then go through a post-processing step that merges the adjacent tracks and cloud areas if the average distance between two tracks is less than 100 km during the same time period. In the final step, we exclude from the analysis the MCS tracks with their lengths below the 25th percentile of the track lengths in observation and in AM4. These two post-processing steps intend to minimize the MCS overcounting and to focus the study on long-lived and more impactful MCSs.

2.3. Cluster analysis of MCS large-scale forcing patterns

To identify and compare large-scale forcing patterns of MCSs in observation and in AM4, we pool the observed and AM4 MCS events together and perform hierarchical clustering of large-scale circulation anomalies associated with these events. Instead of classifying large-scale forcing of MCSs based solely on spatial patterns, our clustering considers both the spatial and temporal characteristics. Specifically, the classification objects are the normalized daily geopotential anomalies at 500 hPa within 20° – 70°N, 150°E - 80°W, *from day -3 to day 0* (with day 0 being the date of the detected MCS genesis) of all the MCS events. Daily geopotential height anomalies are normalized by the maximum absolute value across the entire domain on each day and weighted by the latitude cosine of each grid point. The normalized and weighted 2D matrices are then realigned into vectors and the vectors on day -3 to day 0 are concatenated into a single vector. This single vector contains key spatiotemporal structures of geopotential height anomalies over four consecutive days prior to MCS genesis and becomes the classification object of clustering.

The hierarchical clustering algorithm adopted here employs Ward's minimum variance to compute the distance between two clusters (Ward 1963; Zhao et al. 2016, 2017; Hu et al. 2019a, b). The first merging occurs when two clusters have the smallest Ward's distance. The same procedure is repeated for the updated group of clusters until there is a significant jump in the smallest Ward's distance from the previous step. This indicates that the two clusters merged at this step have significantly different structures and should not be merged any further. The clustering analysis is thus terminated at the previous step and the number of clusters at the previous step is the final number of clusters. Our analysis identifies 5 groups of large-scale forcing patterns for the observed and modeled MCSs, each characterized by a distinct spatial distribution and temporal growth pattern. Each of these groups, or "mix-clusters," contains MCS events from both observation and the AM4 model. By contrasting the contribution of each mix-cluster to the observed and simulated MCSs respectively, we can evaluate how well AM4 captures the properties of MCS large-scale forcing

compared to observation. Bearing uncertainties of clustering, model-observation discrepancies in MCS characteristics within a single mix-cluster are uniquely attributed to model biases in simulating local dynamic and thermodynamic factors such as fronts and LLJs.

The main rationale for using mix-clustering in this study is to simplify the comparison by pooling together observations and model results, as opposed to analyzing them separately. In the case of separate clustering analysis, we will need to compare multiple aspects of the two sets of clusters, including the total number of clusters, the composite circulation patterns, the number of events in each cluster, and the percentage contribution of each cluster to the total MCS population. Such an expanded scope of comparison would be quite challenging as it is subject to many more uncertainties intrinsic to the clustering algorithm and the model being evaluated. By pooling the AM4 and the observed MCS-related circulation patterns together and conducting mix-clustering, we can focus our comparison on each cluster's relative contribution to the total MCS population, which greatly simplifies the model evaluation.

3. Results

3.1. MCS climatology and its lifecycle characteristics

The algorithm outlined in Section 2.2 detected a total of 1160 MCSs in observation and 951 MCSs in AM4. Further examination shows that the long-term springtime average of T_b in AM4 is one degree higher than that observed within the detection domain (not shown). If we add 1K to both T_b thresholds in detecting AM4 MCSs (i.e., 222 K in the "cold core" threshold and 232 K in the warmer threshold), the number of AM4 MCSs will increase to 1163, aligning closely with the number observed. This indicates a systematic positive bias in modeling MCS-related OLR anomalies and thus a general underestimation of MCS number and intensities. In other words, the simulated convections appear to be less intense and penetrating than those observed. Such biases are tied to model resolution and/or potential deficiencies in the model's parameterization of deep convections. A counterpart analysis of MCSs from a global or regionally refined "cloud-resolving" model should help clarify this point. Moreover, as noted in Section 2.2, the post-processed MCS database exclusively encompasses long-lived MCSs. The intensity of short-lived MCSs is also generally weaker in AM4, similar to the pattern observed in long-lived MCSs, which will be discussed later (Fig. 3a). However, given that short-lived MCSs contribute minimally to seasonal precipitation in comparison to their long-lived counterparts (Feng et al. 2019, YD22), they are of trivial importance and thus fall outside the scope of this study.

In addition to the underestimation of MCS occurrence frequency in AM4, the spatial distribution of the MCS track density and activity in AM4 is also markedly different from that in observation (Fig. 1). For the track density (Fig. 1a, b), we separate the entire detection domain into 0.25° × 0.25° pixels and count the number of MCS track points (the locations of MCS centers) falling into each pixel. The activity maps (Fig. 1d, e) are generated from each MCS' intensity on all the associated cloud pixels (intensity at each pixel is defined as the difference between the warmer T_b threshold and the actual T_b of the pixel). During the period of 2000-2014, the track density and activity of springtime MCSs peak over the Southern Great Plains (SGP) in observation (Fig. 1a, d), which is consistent with results from previous studies (e.g., Cui et al. 2020; Tian et al. 2020). In contrast, the maximum MCS track density in AM4 is found over the southern Midwest, and the overall MCS activity is shifted further eastward in comparison to the observation

(Fig. 1b, e). These biases are more evidently revealed by the zonally-oriented dipoles ("negative-positive") in the model-observation differences of the normalized MCS track density and activity (Fig. 1c, f). This pattern is consistent with the results in Dong et al. (2023), which reports a significant overestimation of MCSs in AM4 over the eastern U.S. using a different MCS detection algorithm. The eastward drifting of active MCS zones over the U.S. has also been documented in many other GCMs (e.g., Ferraro et al. 2017; Lin et al. 2022), suggesting a cause more fundamental than resolution and physical parameterizations that tend to vary across models.

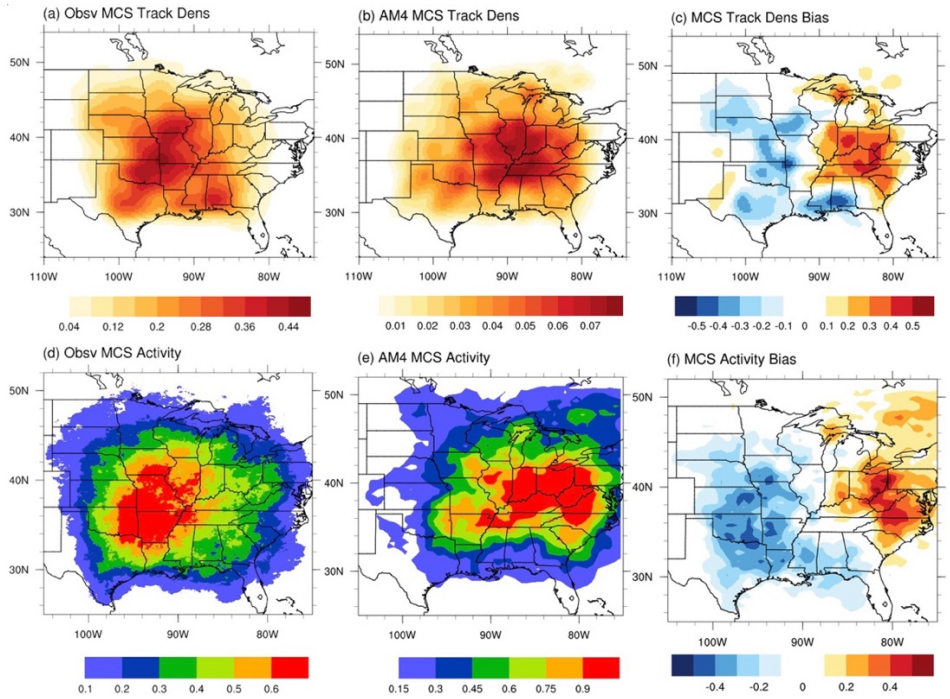

Fig. 1 The climatological MCS track density in observation (a) and in AM4 (b), and the normalized bias of track density (c). The climatological MCS activity (K) (defined as $231K–T_b$ at each pixel within MCS cloud area) in observation (d) and in AM4 (e), and the normalized bias of MCS activity (f)

MCSs play the most important role in the hydrological cycle over the central U.S. in warm season. Figure 2 illustrates the total springtime precipitation (top row), MCS-related precipitation (middle row) and the 95th percentile of daily precipitation rate (bottom row) over the region. The left, middle and right columns correspond to observation, AM4 simulation, and AM4-observation difference (model bias), respectively. The calculation of observational precipitation is based on the Climate Prediction Center (CPC) global gridded daily precipitation data. In general, AM4 overestimates the precipitation amount in spring, featuring a pronounced wet bias over the Great Lakes region/eastern U.S. and a weak dry bias near the Gulf coast in the southern U.S. (Fig. 2a-c). The distribution of extreme precipitation rate (quantified by the 95th percentile of the daily precipitation rate) and the corresponding AM4 bias is similar to that of the spring total (Fig. 2g-i). Unlike previous evaluations of other GCMs (e.g., Feng et al. 2021), AM4 does not exhibit an overall dry bias over the central U.S., especially over the Northern Great Plains (NGP) (Fig. 2c). This feature is also present in extreme precipitation (Fig. 2i). Observational MCSs contribute to more than 60% of springtime precipitation over the SGP (Fig. 2d), a finding consistent with prior studies (e.g., Feng et al. 2019; Cui et al. 2020). Nevertheless, a significant negative bias in the MCS precipitation is evident over the Great Plains (Fig. 2f).

Lack of MCS activity in GCMs has long been linked to the underestimation of warm season precipitation (e.g., Klein et al. 2006; Van Weverberg et al. 2018). In AM4, the underestimation of MCS activity clearly accounts for part of the overall dry bias over the SGP, but over the Central and Northern Great Plains (Fig. 2c), the lack of precipitation due to a lack of MCS activity is overcompensated by extra precipitation associated with other weather systems (e.g., stratiform precipitation in extratropical cyclones; figures now shown), leading to a weak wet bias in the region. MCSs are thus responsible for a smaller portion of the total precipitation in AM4 compared to observation.

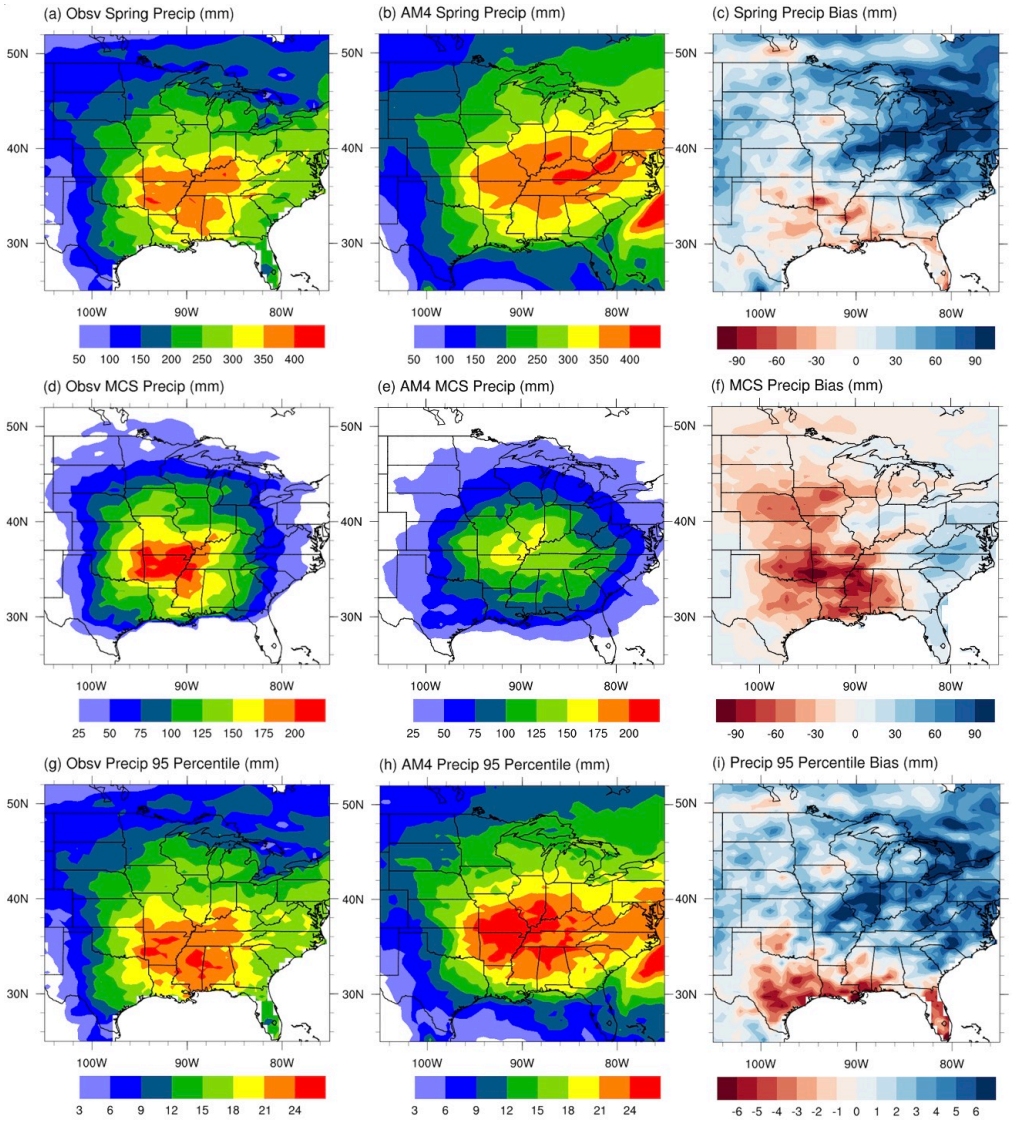

Fig. 2 The total springtime precipitation (mm) in observation (a), in AM4 (b) and its AM4 bias (c). The springtime MCS precipitation in observation (d), in AM4 (e), and its AM4 bias (f). The 95th percentile of springtime daily precipitation rate (mm/day) in observation (g), in AM4 (h), and its AM4 bias (i)

Figure 3 offers a comparison of multiple properties between the observed and modeled MCSs presented as probability density functions (PDFs). Generally, MCSs in AM4 exhibit weaker intensities (quantified by the difference between 231K and the minimum T_b during the MCS lifecycle) compared to those in observation (Fig. 3a), consistent with an overall overestimation of OLR and T_b over the central U.S. discussed earlier. The total precipitation and

maximum precipitation rate of individual MCSs, however, tend to be greater in AM4 than in observation (Figs. 3c and 3d). Specifically, AM4 generates more MCS events with a maximum precipitation rate of 40-75 mm/day and fewer events with a maximum precipitation rate below 40 mm/day (Fig. 3d). The PDFs of the MCS duration are shown in Figure 3b, highlighting the tendency of AM4 to produce more long-lasting (>11 hours) MCSs than observation despite simulating weaker intensities.

Figure 4 displays scatter plots and corresponding third-order polynomial curve fittings for variables characterizing MCS properties. Both the MCS total precipitation (Fig. 4a) and maximum precipitation (Fig. 4b) increase with the maximum MCS (convective) intensity in general. Such increases are much more pronounced in AM4, as indicated by the larger "slopes" of the fitted red curves. This contrast in "precipitation vs. intensity" sensitivity suggests that convective precipitation likely contributes more to MCS precipitation in AM4 while stratiform precipitation is underrepresented. Such biases represent a long-standing issue in GCMs, often attributed to deficiencies in model microphysics schemes (e.g., Morrison et al. 2009; Barnes and Houze Jr. 2016). To summarize, MCSs are in general weaker, wetter, longer-lasting, and more convective-driven in the AM4 model. Many other GCMs produce MCSs with similar characteristics (e.g., Feng et al. 2021; Dong et al. 2021; Lin et al. 2022), but it remains unclear if the identified biases come from a similar source such as problems in a particular model physics scheme.

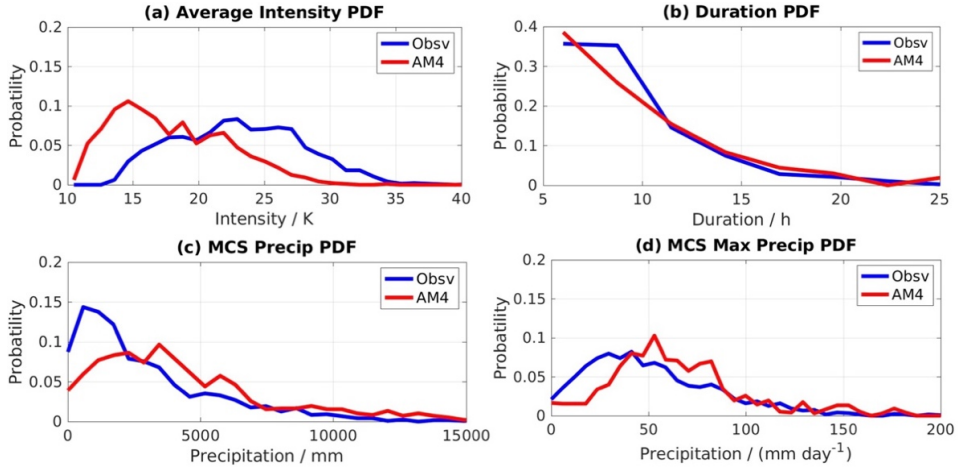

Fig. 3 The probability density function of maximum MCS intensity (K) (a), MCS duration (h) (b), MCS precipitation (mm) (c), and maximum MCS precipitation rate (mm/day) (d) in observation (blue) and in AM4 (red)

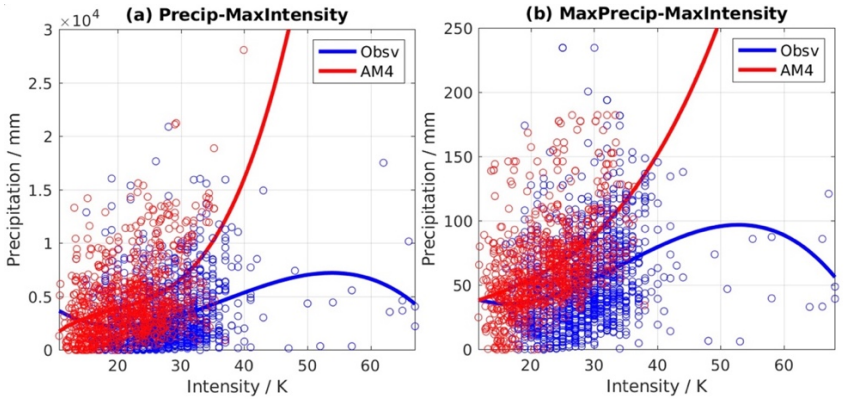

Fig. 4 Scatter plots and regression lines of individual MCS precipitation (mm) - maximum intensity (K) (a) and maximum precipitation rate (mm/day) - maximum intensity (K) (b), for observational (blue) and AM4 (red) events

3.2. Large-scale forcing of MCS genesis

Following You and Deng (2023), we adopt hierarchical clustering to classify the large-scale circulation anomalies preceding MCS genesis in both observation and AM4. As discussed in Section 2.3, the daily 500 hPa geopotential height anomalies from day -3 to day 0 of MCS genesis from both AM4 and observation are pooled together to form the classification objects. Hierarchical clustering applied to this pool of geopotential height anomalies (corresponding to a total of MCS 2111 events) identifies 5 distinct mix-clusters, which is ranked based on the number of MCS events in each cluster (601, 529, 404, 324, and 253 events in Cluster 1 to 5, respectively). Each cluster encompasses a mixture of AM4 and observed MCS events sharing a very similar large-scale forcing pattern. The contribution of each cluster to the total number of events, separately for the model (red bars) and observation (blue bars), is shown in Figure 5. Notably, the percentage contribution of each mix-cluster to the total AM4 and observational MCS population is comparable across all clusters. AM4 is thus capable of representing in general the characteristics of large-scale circulation anomalies leading to MCS development. This is quite encouraging as many GCMs have struggled to simulate these forcing mechanisms accurately (e.g., Song et al. 2019). This finding also bolsters our confidence in AM4's ability to simulate both short-term fluctuations and long-term trends of MCSs over the continental U.S.

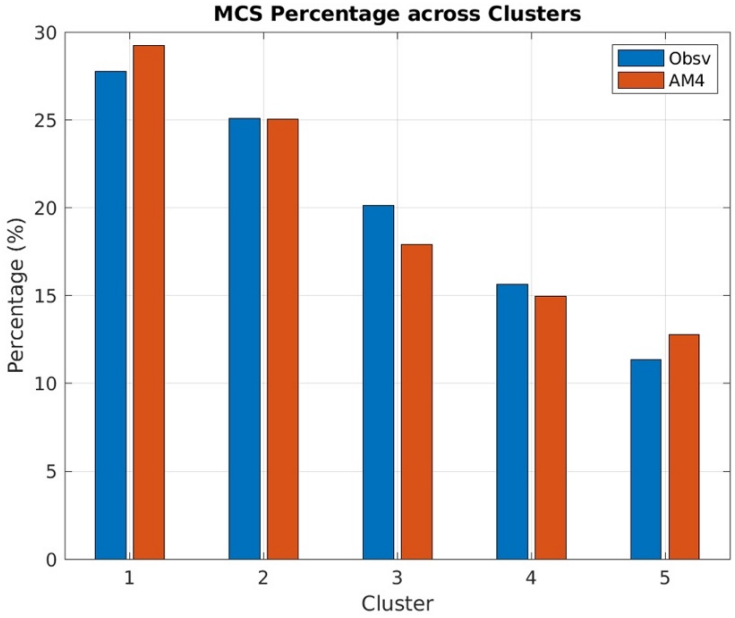

Fig. 5 Percentage contribution (%) of each mix cluster to observational (blue bars) and to AM4 (red bars) MCS events, respectively

Figure 6 displays the composite 500 hPa geopotential height anomalies (contours) for each mix-cluster and the AM4 bias of MCS track density (color shading) within each cluster. Most of these composite height anomalies resemble the patterns previously identified for observed MCS events in spring, roughly aligning with two categories: "remotely forced" and "locally excited", based upon the source region of disturbances (YD22). Cluster 1 is characterized by a quasi-stationary wave train extending from the subtropical western North Pacific into western North America and an amplifying ridge over the southeastern U.S. due to downstream energy propagation. Cluster 2 features

a cutoff low residing near the Gulf of Alaska and a rapidly intensifying low pressure near the southwest U.S. (similar to Cluster 4 in YD22). In Cluster 3, a low-pressure anomaly is situated near the U.S. west coast, gradually migrating inland and triggering MCSs on day 0 (similar to Cluster 1 in YD22). In Cluster 4, a zonally elongated positive height anomaly occupies the central North Pacific, accompanied by the downstream growth of a negative anomaly with a large meridional extent (similar to Cluster 3 in YD22). Cluster 5 includes a intense positive anomaly over the Gulf of Alaska and a pronounced, zonally extended negative anomaly occupying the central North Pacific and the western Canada (similar to Cluster 5 in YD22). In summary, AM4 captures two "locally excited" patterns (Clusters 2 and 3) and two of the "remotely forced" patterns (Clusters 4 and 5) observed. However, it fails to replicate one "remotely forced" pattern (Cluster 2 in YD22), characterized by synoptic disturbances propagating downstream towards North America from the North Pacific storm track. The missing pattern has been demonstrated to be responsible for the observed positive trend of MCS genesis frequency from 2000 to 2020 (YD22), which is not evident in observation and in AM4 for the 2000-2014 period investigated here. This suggests that the downstream modulation of the U.S. MCS activity by the Pacific storm track likely strengthens after 2014, resulted from the phase transition of the Pacific Decadal Oscillation (PDO, see discussions in YD22).

The dipole structures of the MCS track density in Figure 6 (the last figure of each row) indicate that the AM4 bias in MCS activity (i.e., an eastward shift of the maximum track density) is present in all mix-clusters. This result is consistent with previous findings that while large-scale forcing triggers MCS genesis, it has only limited influences on the tracking and lifecycle details of MCSs (YD22). Any factors responsible for such locational biases, whether internal or external, appear to be active across all large-scale forcing patterns. Since local dynamic and thermodynamic processes, such as fronts and moisture convergence associated with LLJs, largely determine the MCS genesis location within an "envelope" associated with a particular large-scale forcing pattern (YD22), the following section will investigate the AM4 biases in these local factors and examine their potential connections to the biases in MCS location.

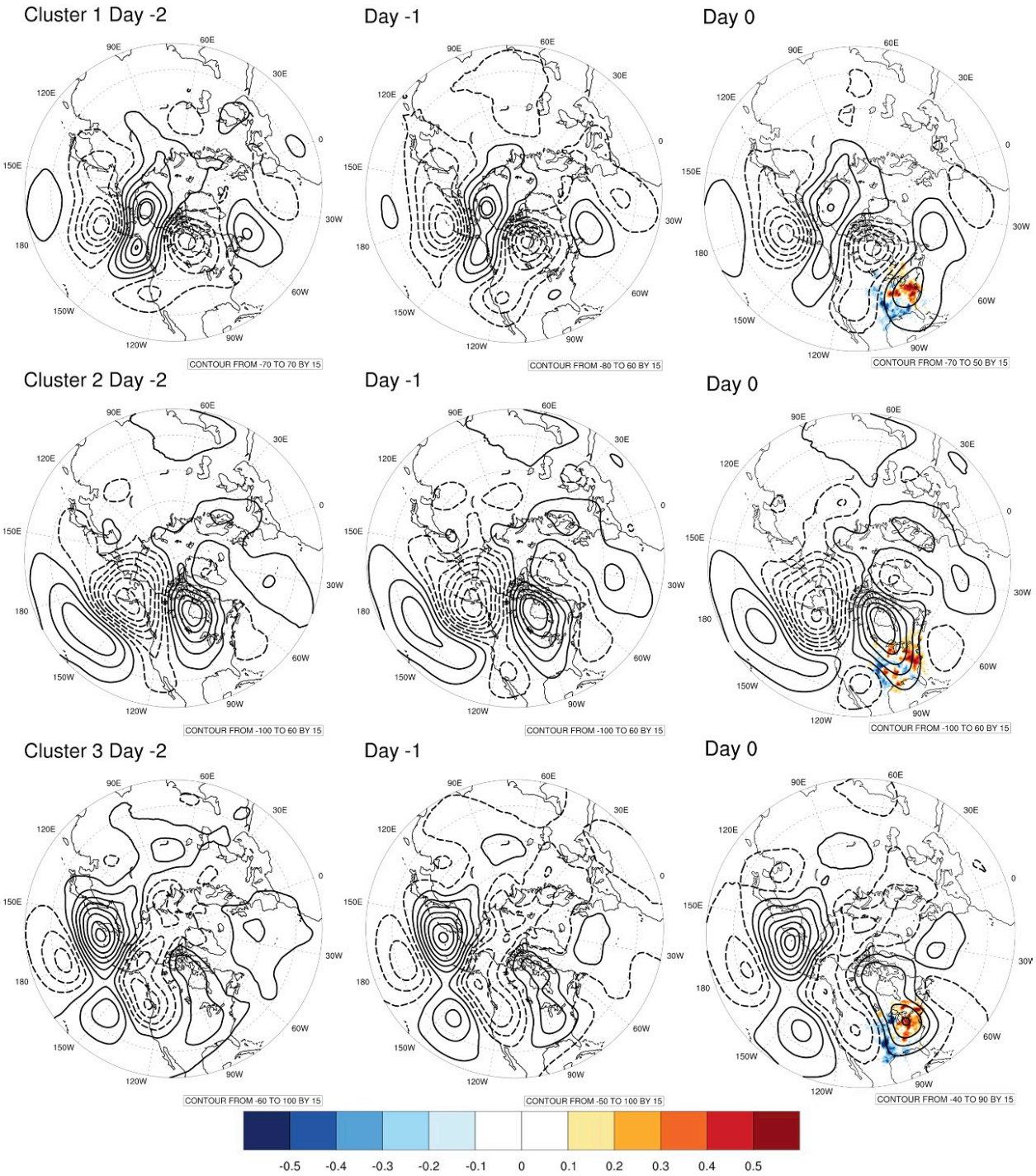

Fig. 6 The composite daily 500 hPa geopotential height anomalies (contour; gpm) on day -2 to day 0 of MCS genesis in Clusters 1, 2, 3 obtained from the classification of large-scale forcing of MCSs. The contour has an interval of 15, with positive values in solid lines and negative values in dashed lines. Each row displays the evolution of circulation anomalies for one cluster. Color shading in the last figures of each row means the bias of normalized MCS activity in each cluster

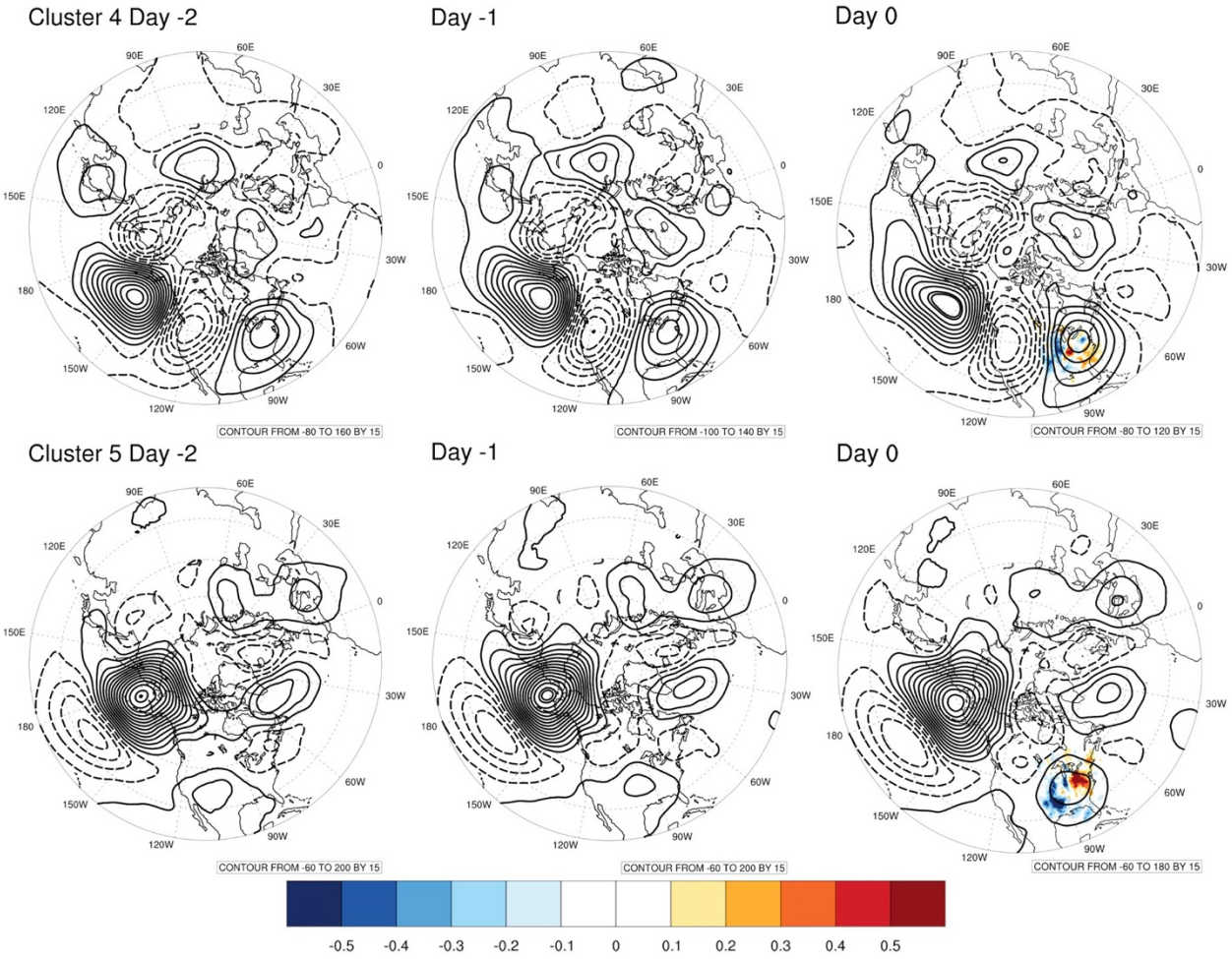

Fig. 6 (continued) For Clusters 4-5

3.3 Local processes contributing to the MCS location biases

Figure 7 displays the sea level pressure (SLP, color shading) and the surface temperature (contours) anomalies on the day of MCS genesis in both observation and AM4. The SLP anomalies help identify synoptic weather systems such as extratropical cyclones, the "parent storms" of most springtime MCSs. Large surface temperature gradients indicate the presence of synoptic-mesoscale fronts (denoted by the red lines in Fig. 7) that provide the necessary lifting for convection initiation, in addition to the large-scale ascent driven by upper-level troughs. In AM4, the low-pressure systems (i.e., cyclones) are weaker compared to the observed, while a stronger high-pressure anomaly builds up along the east coast of the U.S. The fronts (red lines) accompanying the cyclones shift eastward compared to those in observation. Since springtime MCSs tend to initiate ahead of surface cold fronts in the warm sector of extratropical cyclones (YD22), biases in cyclone properties, particularly the front locations, have likely contributed to the eastward shift of MCS activity in AM4 (Fig. 1).

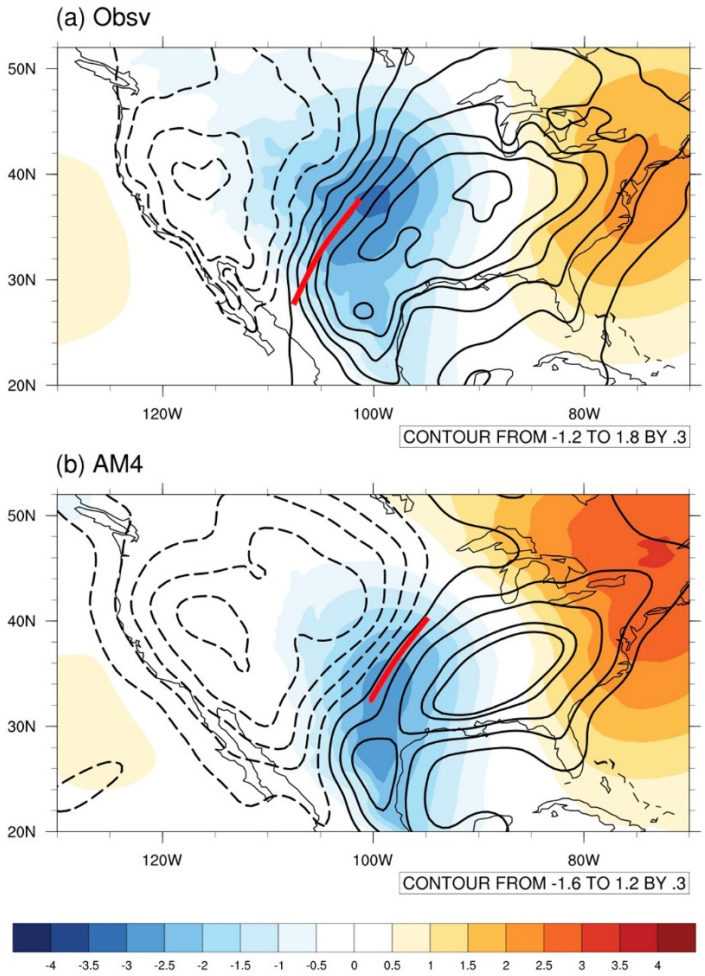

Fig. 7 Surface temperature (contour; K) and sea level pressure anomalies (color shading; hPa) on MCS genesis day in observation (a) and AM4 (b). The red lines in (a) and (b) denote the average front locations characterized by the area of the largest temperature gradients. The contour has an interval of 0.3, with positive values in solid lines and negative values in dashed lines

In addition to the surface variables, moisture transport at 850 hPa best captures the dynamic (low-level convergence) and thermodynamic effects of LLJs on MCS development. Typically, large-scale mechanical lifting to the east of the Rocky Mountains triggers MCSs over the Great Plains while LLJs over the SGP carry moisture northward into the MCS genesis region (e.g., Trier and Parsons 1993). The impact of LLJs, however, is underestimated in AM4, characterized by a northerly bias of LLJ moisture transport over the Great Plains on the day of MCS genesis (Fig. 8, vectors). The negative bias of MCS track density (Fig. 8, color shading) overlaps with a divergent bias of moisture transport (Fig. 8, contours), highlighting the significance of LLJ moisture transport in determining the precise locations of MCSs. Therefore, AM4's underrepresentation of LLJs is another important contributor to the MCS location biases. It is important to note that, in discussing various local dynamic and thermodynamic factors contributing to the locational biases of MCSs, we refrain from identifying a dominant factor. Wang et al. (2019) present an intriguing perspective by exploring this issue through the classification of local meteorological regimes and offer insights into the connection between precipitation biases and the diurnal cycle and the associated precipitation

types. However, quantifying the relative importance of a particular local factor in driving MCS locational biases in the context of our analysis requires further work (e.g., global model experiments with local factors controlled), and this is beyond the scope of the present study.

The development of the Great Plains LLJs is known to be closely coupled with the lifecycles of MCSs (e.g., Trier and Parsons 1993; Dai et al. 1999; Carbone et al. 2002; Feng et al. 2016), implying that weaker LLJs seen in AM4 may partly stem from suppressed MCS activity in the region. However, the weakened Great Plains LLJs documented here have a fundamental origin. As shown in Figure 9a, the seasonal mean (spring average) SLP in AM4 demonstrates a low-pressure bias over the eastern North America and a high-pressure bias over the subtropical North Atlantic. The negative bias of the 850 hPa streamfunction over North America is dynamically consistent with the northerly bias of LLJ moisture transport revealed in Figure 8. It is important to note that this pattern of SLP bias, i.e., negative biases over land and positive biases over subtropical oceans, is widespread across the entire Northern Hemisphere (e.g., positive values over the western North Pacific and negative values over the Eurasian continent). Such a bias pattern is clearly present on days when MCS occurs (Fig. 9b), suggesting that the biases in seasonal mean circulation contribute at least partially to the weakened Great Plains LLJs in AM4 (Fig. 8), consequently influencing the eastward-shifted MCS activity in the model.

The systematic negative SLP bias over land and positive bias over subtropical oceans likely arise from the absence of two-way air-sea interactions in the AM4 experiments evaluated. In reality or in a fully coupled model, at locations characterized by climatological large-scale descent such as the North Atlantic subtropical high, clear sky induces excessive shortwave heating of the surface, elevating surface and lower-tropospheric temperatures. This process diverts air mass out of the column and subsequently weakens the initial surface high pressure. Such a negative feedback mechanism, dynamically marked by the generation of a positive low-level potential vorticity (PV) anomaly, is missing when the SST is prescribed and fixed in a model. Consequently, this results in a positive SLP bias over the subtropical highs and negative SLP biases over adjacent lands due to large-scale mass conservation. Such mechanisms have been argued to be responsible for the model biases in the climatological location of the East Asian monsoonal fronts (Li et al. 2018, 2019). It is noteworthy that the eastward shift of MCS activity over the continental U.S. is also observed in many other atmosphere-only GCMs (Ferraro et al. 2017; Lin et al. 2022), suggesting that the mechanism proposed here likely serves as a fundamental cause of such “location bias” of MCS activity.

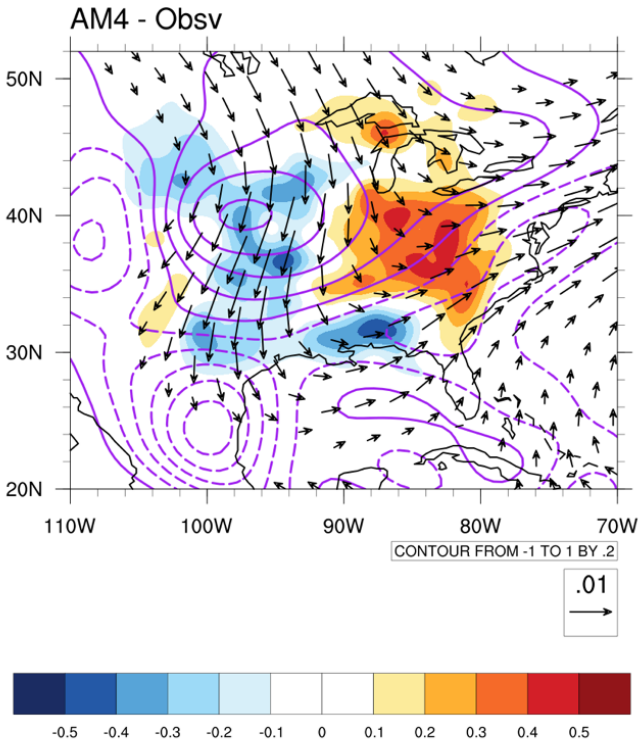

Fig. 8 AM4 bias of normalized track density (as in Figure 1c; color shading), 850 hPa water vapor transport (vector; m/s), and its divergence (contour; 10^{-8} s^{-1}) during MCS days. The contour has an interval of 0.2, with positive values in solid lines and negative values in dashed lines

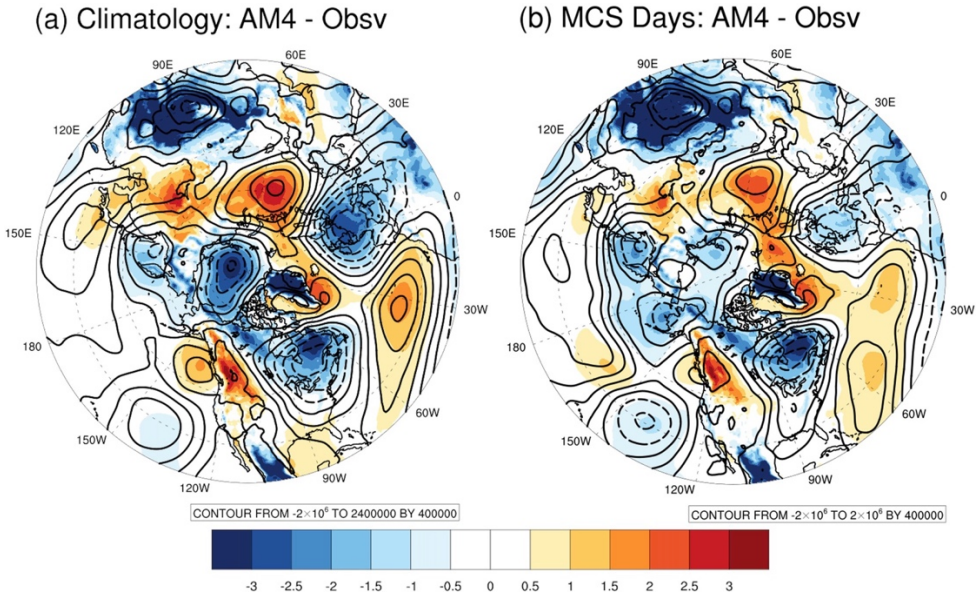

Fig. 9 AM4 bias of 850 hPa streamfunction (contour; m^2 s^{-1}) and sea level pressure (color shading; hPa) in (a) springtime climatology and in (b) MCS days

4. Conclusion and discussion

This study presents a comprehensive evaluation of the GFDL AM4's performance in simulating the springtime U.S. MCSs, their associated precipitation, and the multiscale forcing mechanisms regulating MCS lifecycle

characteristics. Our analysis identifies a smaller number of MCSs in AM4 due to a systematic error in modeling OLR and T_b within the detection domain. AM4 also demonstrates significant bias in the location of MCS activity, with the peak of the MCS track density shifting from the SGP in observation to the Midwest in AM4. This displacement of MCS activity is directly responsible for an eastward shift of the MCS precipitation. The contribution of such a shift to the seasonal precipitation bias is however limited due to the compensation by the enhanced extratropical cyclone activity over the central U.S., particularly the NGP. Moreover, MCSs in AM4 are less intense but longer-lasting and producing more precipitation compared to the observed ones. Deep convective rainfall accounts for a much greater portion of the total MCS rainfall in the AM4 model, in agreement with the broader challenge in simulating MCS stratiform precipitation.

Despite the obvious biases in the simulated MCS locations and precipitation properties, it is encouraging to see that the AM4 model captures the large-scale forcing patterns of MCSs in terms of the spatiotemporal features and the relative contributions of individual circulation anomalies. The successful representation of the springtime planetary and synoptic environments spawning MCSs bolsters confidence in using AM4 to conduct short-term predictions (e.g., subseasonal-to-seasonal) and long-term projections (e.g., externally forced trends) for MCS-related weather hazards. Specifically, hierarchical clustering based on pooled model and observed MCS circulation anomalies yields large-scale forcing patterns resembling those classified solely from the observed MCS circulation anomalies. These patterns can also be divided into two groups - “remotely forced” and “locally excited” based upon their dynamical origins.

To understand the MCS location bias present under different large-scale forcing patterns, we delve into local dynamic and thermodynamic factors that play more important roles in MCS tracking and lifecycle characteristics. Weaker surface lows (cyclones), eastward shifted fronts, and significantly subdued Great Plains LLJs moisture transport are found to be key factors contributing to the suppression of MCS activity over the Great Plains and the relatively enhanced MCS activity over the Midwest. It is further argued that the eastward shift of MCS activity in AM4 is driven by biases in both the seasonal mean circulation and synoptic-mesoscale anomalies. Specifically, the prescribed-SST AM4 simulations, lacking the atmospheric feedback to SST, result in a positive pressure bias in the North Atlantic subtropical high. Following mass conservation, this positive SLP bias results in a pronounced negative SLP bias over much of the eastern U.S. and generates a seasonal mean northerly bias over the Great Plains that consequently weakens the LLJ and its northward moisture transport. This synergy between biases in seasonal mean circulation and biases in synoptic-mesoscale anomalies (i.e., weaker cyclone and shifted fronts) drives the eastward shift of MCS activity from the Great Plains to the Midwest.

However, it is essential to note that all factors responsible for the modeled MCS biases identified here are dynamically coupled with the lifecycles of MCSs. Delineating the exact causality for a quantitative attribution of the biases demands further evaluations of carefully designed model experiments that isolate the process-level impacts of multiple factors. These include model physical parameterization schemes which are not the focus of the present study. Finally, it is worth highlighting that the seasonal mean SLP bias identified here, an unintended consequence of the prescribed-SST setup, suggests that extra caution should be taken when making use of the extended-range forecasts of MCSs, where SSTs tend to be fixed in the forecast models.

Acknowledgement

The authors would like to thank two anonymous reviewers for their constructive comments that led to significant improvement of the paper. This study is support by the U.S. National Science Foundation (NSF) through Grant AGS-2032532 and by the U.S. National Oceanic and Atmospheric Administration (NOAA) through Grant NA22OAR4310606. Deng is also partly supported by the NOAA through Grant NA20OAR4310380.

Data availability statement

The GFDL AM4 data are obtained from collaborations with Wenhao Dong affiliated at GFDL and Yi Ming affiliated at Boston College. The global merged geostationary satellite infrared brightness temperature dataset is produced by the NOAA Climate Prediction Center and archived at the NASA Goddard Earth Sciences Data and Information Services Center (GES DISC) at https://disc.gsfc.nasa.gov/ datasets/GPM_MERGIR_1/summary. The observational precipitation comes from the Climate Prediction Center (CPC) global gridded daily precipitation data (https://psl.noaa.gov/data/gridded/data.cpc.globalprecip.html). The atmospheric variables on the single level and all pressure levels come from the fifth generation of ECMWF reanalysis dataset (ERA5) and are available on the Climate Data Store (https://cds.climate. copernicus.eu/#!/search?text=ERA5&type=dataset).

Declaration

Conflict of Interest We declare that we have no conflict of interest.

References

Barnes HC, Houze Jr. RA (2016) Comparison of observed and simulated spatial patterns of ice microphysical processes in tropical oceanic mesoscale convective systems. Journal of Geophysical Research: Atmospheres 121:8269–8296. https://doi.org/10.1002/2016JD025074

Carbone RE, Tuttle JD, Ahijevych DA, Trier SB (2002) Inferences of Predictability Associated with Warm Season Precipitation Episodes. Journal of the Atmospheric Sciences 59:2033–2056. https://doi.org/10.1175/1520-0469(2002)059<2033:IOPAWW>2.0.CO;2

Cui W, Dong X, Xi B, et al (2020) Can the GPM IMERG Final Product Accurately Represent MCSs' Precipitation Characteristics over the Central and Eastern United States? Journal of Hydrometeorology 21:39–57. https://doi.org/10.1175/JHM-D-19-0123.1

Dai A, Giorgi F, Trenberth KE (1999) Observed and model-simulated diurnal cycles of precipitation over the contiguous United States. Journal of Geophysical Research: Atmospheres 104:6377–6402. https://doi.org/10.1029/98JD02720

Dong W, Zhao M, Ming Y, et al (2023) Simulation of United States Mesoscale Convective Systems Using GFDL's New High-Resolution General Circulation Model. Journal of Climate 1:1–40. https://doi.org/10.1175/JCLI-D-22-0529.1

Dong W, Zhao M, Ming Y, Ramaswamy V (2021) Representation of Tropical Mesoscale Convective Systems in a General Circulation Model: Climatology and Response to Global Warming. Journal of Climate 34:5657–5671. https://doi.org/10.1175/JCLI-D-20-0535.1

Ellingson RG, Ferrado RR (1983) An Examination of a Technique for Estimating the Longwave Radiation Budget from Satellite Radiance Observations. Journal of Applied Meteorology and Climatology 22:1416–1423. https://doi.org/10.1175/1520-0450(1983)022<1416:AEOATF>2.0.CO;2

Feng Z, Houze RA, Leung LR, et al (2019) Spatiotemporal Characteristics and Large-Scale Environments of Mesoscale Convective Systems East of the Rocky Mountains. Journal of Climate 32:7303–7328. https://doi.org/10.1175/JCLI-D-19-0137.1

Feng Z, Leung LR, Hagos S, et al (2016) More frequent intense and long-lived storms dominate the springtime trend in central US rainfall. Nat Commun 7:13429. https://doi.org/10.1038/ncomms13429

Feng Z, Leung LR, Houze Jr. RA, et al (2018) Structure and Evolution of Mesoscale Convective Systems: Sensitivity to Cloud Microphysics in Convection-Permitting Simulations Over the United States. Journal of Advances in Modeling Earth Systems 10:1470–1494. https://doi.org/10.1029/2018MS001305

Feng Z, Song F, Sakaguchi K, Leung LR (2021) Evaluation of Mesoscale Convective Systems in Climate Simulations: Methodological Development and Results from MPAS-CAM over the United States. Journal of Climate 34:2611–2633. https://doi.org/10.1175/JCLI-D-20-0136.1

Ferraro R, Waliser D, Peters-Lidard C (2017) NASA downscaling project: final report. Pasadena, CA: Jet Propulsion Laboratory, National Aeronautics and Space Administration, 2017

Haberlie AM, Ashley WS (2019) A Radar-Based Climatology of Mesoscale Convective Systems in the United States. Journal of Climate 32:1591–1606. https://doi.org/10.1175/JCLI-D-18-0559.1

Houze RA (2018) 100 Years of Research on Mesoscale Convective Systems. Meteorological Monographs 59:17.1-17.54. https://doi.org/10.1175/AMSMONOGRAPHS-D-18-0001.1

Hu Y, Deng Y, Zhou Z, et al (2019a) A statistical and dynamical characterization of large-scale circulation patterns associated with summer extreme precipitation over the middle reaches of Yangtze river. Clim Dyn 52:6213–6228. https://doi.org/10.1007/s00382-018-4501-z

Hu Y, Deng Y, Zhou Z, et al (2019b) A synoptic assessment of the summer extreme rainfall over the middle reaches of Yangtze River in CMIP5 models. Clim Dyn 53:2133–2146. https://doi.org/10.1007/s00382-019-04803-3

Janowiak JE, Joyce RJ, Yarosh Y (2001) A Real-Time Global Half-Hourly Pixel-Resolution Infrared Dataset and Its Applications. Bulletin of the American Meteorological Society 82:205–218. https://doi.org/10.1175/1520-0477(2001)082<0205:ARTGHH>2.3.CO;2

Klein SA, Jiang X, Boyle J, et al (2006) Diagnosis of the summertime warm and dry bias over the U.S. Southern Great Plains in the GFDL climate model using a weather forecasting approach. Geophysical Research Letters 33:. https://doi.org/10.1029/2006GL027567

Li Y, Deng Y, Yang S, et al (2019) Multi-scale temporal-spatial variability of the East Asian summer monsoon frontal system: observation versus its representation in the GFDL HiRAM. Clim Dyn 52:6787–6798. https://doi.org/10.1007/s00382-018-4546-z

Li Y, Deng Y, Yang S, Zhang H (2018) Multi-scale temporospatial variability of the East Asian Meiyu-Baiu fronts: characterization with a suite of new objective indices. Clim Dyn 51:1659–1670. https://doi.org/10.1007/s00382-017-3975-4

Lin G, Jones CR, Leung LR, et al (2022) Mesoscale Convective Systems in a Superparameterized E3SM Simulation at High Resolution. Journal of Advances in Modeling Earth Systems 14:e2021MS002660. https://doi.org/10.1029/2021MS002660

Lin Y, Dong W, Zhang M, et al (2017) Causes of model dry and warm bias over central U.S. and impact on climate projections. Nat Commun 8:881. https://doi.org/10.1038/s41467-017-01040-2

Mapes B, Tulich S, Lin J, Zuidema P (2006) The mesoscale convection life cycle: Building block or prototype for large-scale tropical waves? Dynamics of Atmospheres and Oceans 42:3–29. https://doi.org/10.1016/j.dynatmoce.2006.03.003

Moncrieff MW, Liu C, Bogenschutz P (2017) Simulation, Modeling, and Dynamically Based Parameterization of Organized Tropical Convection for Global Climate Models. Journal of the Atmospheric Sciences 74:1363–1380. https://doi.org/10.1175/JAS-D-16-0166.1

Morrison H, Thompson G, Tatarskii V (2009) Impact of Cloud Microphysics on the Development of Trailing Stratiform Precipitation in a Simulated Squall Line: Comparison of One- and Two-Moment Schemes. Monthly Weather Review 137:991–1007. https://doi.org/10.1175/2008MWR2556.1

Prein AF, Liu C, Ikeda K, et al (2017) Increased rainfall volume from future convective storms in the US. Nature Clim Change 7:880–884. https://doi.org/10.1038/s41558-017-0007-7

Randall D, DeMott C, Stan C, et al (2016) Simulations of the Tropical General Circulation with a Multiscale Global Model. Meteorological Monographs 56:15.1-15.15. https://doi.org/10.1175/AMSMONOGRAPHS-D-15-0016.1

Schumacher RS, Johnson RH (2006) Characteristics of U.S. Extreme Rain Events during 1999–2003. Weather and Forecasting 21:69–85. https://doi.org/10.1175/WAF900.1

Song F, Feng Z, Leung LR, et al (2019) Contrasting Spring and Summer Large-Scale Environments Associated with Mesoscale Convective Systems over the U.S. Great Plains. Journal of Climate 32:6749–6767. https://doi.org/10.1175/JCLI-D-18-0839.1

Tian J, Dong X, Xi B, Feng Z (2020) Characteristics of Ice Cloud–Precipitation of Warm Season Mesoscale Convective Systems over the Great Plains. Journal of Hydrometeorology 21:317–334. https://doi.org/10.1175/JHM-D-19-0176.1

Trier SB, Parsons DB (1993) Evolution of Environmental Conditions Preceding the Development of a Nocturnal Mesoscale Convective Complex. Monthly Weather Review 121:1078–1098. https://doi.org/10.1175/1520-0493(1993)121<1078:EOECPT>2.0.CO;2

Van Weverberg K, Morcrette CJ, Petch J, et al (2018) CAUSES: Attribution of Surface Radiation Biases in NWP and Climate Models near the U.S. Southern Great Plains. Journal of Geophysical Research: Atmospheres 123:3612–3644. https://doi.org/10.1002/2017JD027188

Wang J, Dong X, Kennedy A, et al (2019) A Regime-Based Evaluation of Southern and Northern Great Plains Warm-Season Precipitation Events in WRF. Weather and Forecasting 34:805–831. https://doi.org/10.1175/WAF-D-19-0025.1

Ward JH (1963) Hierarchical Grouping to Optimize an Objective Function. Journal of the American Statistical Association 58:236–244. https://doi.org/10.1080/01621459.1963.10500845

You Z, Deng Y (2022) A Hierarchical Dissection of Multiscale Forcing on the Springtime Mesoscale Convective Systems in the United States. Journal of Climate 36:39–54. https://doi.org/10.1175/JCLI-D-22-0150.1

Zhao M (2020) Simulations of Atmospheric Rivers, Their Variability, and Response to Global Warming Using GFDL's New High-Resolution General Circulation Model. Journal of Climate 33:10287–10303. https://doi.org/10.1175/JCLI-D-20-0241.1

512 Zhao M, Golaz J-C, Held IM, et al (2018) The GFDL Global Atmosphere and Land Model AM4.0/LM4.0: 1.
513 Simulation Characteristics With Prescribed SSTs. Journal of Advances in Modeling Earth Systems 10:691–
514 734. https://doi.org/10.1002/2017MS001208

515 Zhao S, Deng Y, Black RX (2016) Warm Season Dry Spells in the Central and Eastern United States: Diverging
516 Skill in Climate Model Representation. Journal of Climate 29:5617–5624. https://doi.org/10.1175/JCLI-D-
517 16-0321.1

518 Zhao S, Deng Y, Black RX (2017) A Dynamical and Statistical Characterization of U.S. Extreme Precipitation
519 Events and Their Associated Large-Scale Meteorological Patterns. Journal of Climate 30:1307–1326.
520 https://doi.org/10.1175/JCLI-D-15-0910.1

521